Surfzone currents over irregular bathymetry : Drifter observations and numerical simulations

W. E. Schmidt

Integrative Oceanography Division, Scripps Institution of Oceanography

La Jolla, CA, USA

R. T. Guza

Integrative Oceanography Division, Scripps Institution of Oceanography

La Jolla, CA, USA

D. N. Slinn

Civil and Coastal Engineering Department, University of Florida

Gainesvill, FL 32611-6580

W. E. Schmidt, Integrative Oceanography Division, Scripps Institution of Oceanography, University of California, San Diego. La Jolla, CA 92093-0209. (wschmidt@coast.ucsd.edu)

R. T. Guza, Integrative Oceanography Division, Scripps Institution of Oceanography, University of California, San Diego. La Jolla, CA 92093-0209 (rguza@coast.ucsd.edu)

D. N. Slinn, Civil and Coastal Engineering Department, University of Florida. Gainesville, FL 32611-6580 (slinn@coastal.ufl.edu)

Abstract. Surfzone currents over irregular bathymetry were observed with GPS-tracked drifters, and modeled with the nonlinear shallow water equations. Trajectories of drifters released in 1 to 2 m depth sometimes defined rip currents and surfzone eddies, features that have been difficult to resolve with fixed instruments. The drifter-deliniated surfzone circulation evolved as the tide level changed during each 4-6 hr deployment. In one case, as the tide dropped, a shore-normal rip current present for the first 2 hr evolved to a more shore-parallel flow. In a second case, on a rising tide, a well-developed, bifurcated rip current was replaced by a weak, amorphous circulation. Rip current velocities were strongest near the surfzone edge, and decayed by an order of magnitude within 2 surfzone widths from the shoreline. An eddy was observed to persist over a bathymetric depression within the surfzone for at least 1 hr. Observed and numerically simulated trajectories are qualitatively similar. The observed and modeled velocities differed by roughly a factor of 2, and differences in flow observed during roughly 0.5 m changes in tide level were reproduced only if the simulated water levels varied by about 1 m. The cross-shore momentum balance was dominated by wave-forcing and pressure gradient terms of about equal magntiude and opposite sign. In the vicinity of simulated rip currents, the residual of the forcing and pressure gradient was balanced by nonlinear advection terms. The alongshore momentum balance was also spatially variable, with wave forcing balanced by alongshore pressure gradient, friction, and advective terms.

1. Introduction

Early field observations of surfzone circulation used visually-tracked foam, debris, drifters and dye [e.g., *Hite* 1925, *Shepard et al.* 1941, *Putnam et al.* 1949, and *Shepard and Inman* 1950]. More recent observations of surfzone circulation primarily used fixed arrays of electromagnetic or acoustic current meters [e.g., *Ruessink et al.* 2001 and references therein], in part because of the difficulty in using visual methods. GPS tracking reduces the difficulty of tracking surfzone drifters accurately, and drifter-based observations of surfzone circulation have been reported recently [*Schmidt et al.* 2003, *Johnson and Pattriaratchi* 2004]. Here, a fleet of ten GPS-tracked surfzone drifters are used to describe the evolution of nearshore circulation near an irregularly shaped bar-trough feature in 1 to 2 m water depth.

Surfzone circulation observed on idealized, alongshore-variable laboratory bathymetry is reproduced approximately by numerical simulations that include refraction, depth-dependent wave breaking, and radiation-stress based wave forcing [e.g., *Chen et al* 1999, *Haas and Svendsen* 2002, *Haller et al* 2002, and *Haas et al* 2003]. These experiments suggest that the location of rip currents is controlled by depth-dependent wave breaking on the alongshore-variable bathymetry. Existing field observations confirm the importance of alongshore variable bathymetry to surfzone circulation [e.g., *Sonu* 1972, *Hino* 1974, *Dronen et al* 1999, *Ranasinghe et al* 2000], including at the present study site [e.g., *Shepard and Inman* 1950, *Schmidt et al.* 2003]. Here, we show drifter trajectories suggesting features, including rip currents and surfzone eddies, that are qualitatively similar to predictions of an existing numerical model based on the nonlinear shallow water equations and the observed bathymetry [*Yu and Slinn*, 2003].

2. Study Site and Description of the Observations

Scripps Beach, also known as La Jolla Shores, is located 400 m south of the Scripps Institution of Oceanography (SIO) pier (Figure 1). Aerial photographs predating the present 2-km long seawall backing the beach show a narrow arroyo cutting the low cliff in the proximity of the study site, now the terminus of local drainage from the city storm water grid. In *Shepard and Inman* [1950], rip currents were observed in this area for 4 of the 6 incident wave conditions studied. Recent surveys often show alongshore depth inhomogeneity in the region adjacent to the storm drain outlet, frequently the location of visually observed rip currents.

As reported in *Schmidt et al.* 2003, the tubular PVC body of the drifters is ballasted for nearly complete submergence and a strong righting moment (Figure 2). A PVC disc at the bottom of the body tube dampens the drifter vertical response to rapid changes of water level, allowing broken and near-breaking waves to pass over without rapidly pushing the drifter ashore (i.e., 'surfing'). Each drifter transmits differential-GPS positions (3-5 m accuracy) to shore at 0.1Hz for real-time tracking, and internally records raw GPS data at 1 Hz for non-differential, post-processed GPS positions (sub-meter accuracy).

There were 7 deployments of 5 to 6 hr duration during the period 19-27 July 2001, and 3 deployments of 4 to 5 hr duration one year later, on 29-31 July, 2002. Bathymetry surveys of an approximately 600-m alongshore span, with 25 m spacing between cross-shore transects, were obtained on 18 and 27 July 2001, and on 26 July 2002, with GPS-equipped jetskis and wheeled land vehicles. Tide data was obtained from the SIO pier end (NOAA tide station 9410230). Bathymetry and tide data are presented relative to mean sea level (MSL). Hourly still and time-lapse variance images of the deployment area were obtained from an Oregon State University Coastal Imaging Laboratory (CIL) Argus video camera [*Holland et al*, 1997] (Figure 1 shows

2001 image). Wave conditions immediately offshore (about 7 m MSL) of the observation region were obtained by initializing a refraction model with data from nearby Coastal Data Information Program directional wave buoys (W. O'Reilly, personal communication).

The locations of reference floats (1-2 m depth MSL) were selected based on the bathymetry and visual observations of the circulation. At intervals of about 10-15 min, drifters were manually carried to the reference floats and released, usually in pairs, as directed by personnel at an elevated tracking station. Drifters were retrieved for redeployment when they progressed offshore more than about 2-3 surfzone widths, moved up or downcoast more than about 300 m, or came ashore. Between 40-60 individual drifters were released each day in July 2001, and between 60-80 during each day in July 2002. "Spaghetti" plots for 19 July 2001 and 29 July 2002 (selected for detailed analysis, hereafter refered to as Case 1 and Case 2, respectively) are shown in Figure 3, and for all deployment days in *Schmidt* [2003]. See *Schmidt* [2003] and *Schmidt et al.* [2003] for additional description of the drifters, study site, deployment procedures, and data processing.

2.1. Case 1

The Case 1 deployment was conducted during a 5.6 hr period of falling tide (≈ -0.52 m elevation change, between +0.40 and -0.12 m MSL). Selected Case 1 drifter trajectories show a rip current and an eddy (Figures 4 and 5). The last (magenta) rip current drifter deployed in Figure 4 and the first (red) eddy drifter in Figure 5 were released within 1 min and 1 m of each other. Their initial trajectories are similar, but diverge near (x, y)=(80,-180). Maps of spatially and temporally averaged drifter velocities suggest that the shore-normal rip current was present during the first half of the deployment (Figure 6a,b), but ceased flowing as the tide dropped (Figure 6c,d). Rip current velocity maxima were closely coincident with the seaward edge of

the surfzone, and decayed by an order of magnitude within approximately 2 surfzone widths from the shoreline.

During the last half of the deployment (lowest tide levels) the drifter trajectories define a relatively strong, southward-directed, alongshore current and the counter-clockwise (CCW) eddy (estimated eddy center (x (cross-shore), y (alongshore))=(110,-375) in Figures 5 and 6c,d). Similar to *Schmidt et al.* 2003, the eddy was observed to persist for at least 1 hr entirely within the surfzone, the diameter was estimated at 40 m, and the estimated vorticity magnitude was 0.03 s^{-1}. However, the previously observed eddy (July 2000) rotated in a clockwise (CW) direction. Future papers will focus on surfzone eddy dynamics.

2.2. Case 2

The Case 2 deployment spanned about 4.4 hr of rising tide ($\approx +0.79$ m tidal change, between -0.55 and +0.24 m MSL). Velocities of the first 30 drifters released, over roughly the first half of the deployment (Figure 7a), delineate two shore-oblique flows that form the branches of a bifurcated rip current . The velocity maximum of both branches are located approximately at the seaward edge of the surfzone (red curve in Figures 7a and 8a,b), and the velocities of both branches decay by an order of magnitude approximately 2 surfzone widths from the shoreline. The highest variances are predominantly located within the surfzone, with the major axes of variance roughly orthogonal to the direction of the mean flow (Figure 7a), consistant with high shears and vigorous mixing. The widths of the south (left) and north (right) branches are 20 m and 40 m, respectively, estimated as the flow orthonormal distance between drifter trajectories at the surfzone edge. Simple volumetric calculations using these branch widths, 1.5 m mean depth, and 40 cm s^{-1} flow speed at the surfzone edge result in flow rates of about 12 and 24 m^3 s^{-1} for the south and north branches, respectively. At this rate, a triangular volume, 600 m alongshore

by 150 m cross-shore by 1.5 m vertical, could be exchanged with the nearshore coastal waters in approximately 1 hr, and would require a alongshore and depth-averaged onshore flow of about 4 cm s^{-1} (assuming no net inflow at the lateral boundaries).

Averaged drifter velocities during the second half of Case 2 (higher tide levels), when 33 drifters were released, suggest decreased flow in both branches (Figures 7b and 8c,d). Most mean flows are weak (< 15 cm s^{-1}), and are greater (less) than their respective variances outside (inside) the surfzone. During the last 1.1 hr of the deployment, drifter velocities suggest a weak, amorphous circulation (Figure 8d).

2.3. Case Comparison

In Case 1, the 1.5 m depth contour is roughly shore-parallel for almost 100 m on either side of the observed rip current (Figure 9a). In Case 2, this depth contour was wedge-shaped with the flow branches emanating from both sides of the wedge (Figure 9b). Although 1 year apart, the surfzone bathymetries were similar and smooth (Figure 9c), except along the -1.5 m MSL depth contour in the vicinity of the rips.

Differences in the Case 1 and Case 2 flows (at roughly the same tide level) could result from differences in the bathymetries or the incident waves (wave heights (H_0) and periods (T_p) approximately 0.8 m and 9 s for Case 1, and 0.5 m and 7 s for Case 2, with approximately normal incidence angle (Θ) in both cases). However, variations in the incident wave field during each day were relatively small, ($\Delta H_0 < \pm 0.10$ m in both cases, and similarly small changes in T_p and Θ). The substantial variation of the flow during each Case day suggests that modest (e.g., 0.5 m or less) changes in tidal level, and hence in the effective bathymetry, significantly altered the surfzone circulation. Model results confirm this inference.

3. Model Formulation and Data Comparison

The effects of bathymetry and tidal fluctuations were examined with a numerical model based on the nonlinear shallow water equations with a rigid lid, previously used in studies of time-dependent wave-driven circulation on planar [*Allen et al*, 1996], barred [*Slinn et al.*, 1998], and alongshore varying [*Slinn et al.*, 2000] beach topographies, and also in a rip current modeling study [*Yu and Slinn*, 2003]. The wave-averaged forcing of the circulation by breaking waves [*Longuet-Higgins*, 1970] is modeled with the bore-based model of *Thorton and Guza* [1986]. Dissapation is modelled with nonlinear bottom friction [*Wright and Thompson*, 1983], and lateral mixing is neglected. Finite difference methods are used to solve the depth-integrated, nonlinear shallow-water equations,

$$(hu)_x + (hy)_y = 0 \tag{1}$$

$$u_t + uu_x + vu_y = -\frac{p_x}{\rho} + \tau_x^w - \frac{C_f < |\vec{u}|u >}{h} - \nu\nabla^4 u \tag{2}$$

$$v_t + uv_x + vv_y = -\frac{p_y}{\rho} + \tau_y^w - \frac{C_f < |\vec{u}|v >}{h} - \nu\nabla^4 v \tag{3}$$

where *u* and *v* are the cross-shore and alongshore velocities, respectively, averaged over water depth and wave period, *p* is pressure, ρ is constant water density, (τ_x^w, τ_y^w) are the components of wave forcing, t is time, C_f is a dimensionless friction coefficient (0.01 used here), *h* is the local water depth, and ν is a biharmonic dissipation term added to eliminate small scale numerical disturbances. Wave-current interaction has been shown to significantly reduce the cross-shore extent of rip currents [*Yu and Slinn*, 2003], and is included here. Boundary conditions are along-

shore periodic and require zero cross-shore mass flux at the shoreline and offshore boundaries. The biharmonic dissipation term requires the additional constraints that

$$u_{xx} = v_x = v_{xxx} = 0 \tag{4}$$

at the shoreline and offshore boundaries.

The measured bathymetry is centered in the 500 m (cross-shore) by 1000 m (alongshore) model domain. To satisfy alongshore periodicity, the measured bathymetry is relaxed to an alongshore mean within 50 m of the model lateral boundaries. Extending the alongshore domain to 1500 m did not significantly effect the model results. The shoreward ($<\approx$0.5 m) and deepest ($>\approx$ 6 m) model depth contours are relaxed to shore-parallel. To satisfy mass conservation (1) over practical computational intervals (thereby insuring model convergence), the measured bathymetry was smoothed, especially in less than 1 m depth MSL. Smoothing of the bathymetry in depths greater than 1 m MSL was limited, and the measured and model bathymetries are similar, especially between the 0.5 m and 4.5 m contours (MSL) (Figure 10). Numerical results for tide levels less than MSL are not shown because the model sensitivity to bathymetric irregularities in very shallow depths required excessive smoothing of features in 1.5 m depth MSL. The effects of changing water depth were examined (for both cases) by comparing model results at 4 discrete tide levels : MSL, MSL + 0.34 m, MSL + 0.68 m, and MSL + 1.02 m. For each additional 0.34 m of water depth above MSL, a section of constant cross-shore slope (0.017, similar to the observed slope) was added at the shoreline, shifting the MSL bathymetry seaward by 20m. The highest water level observed in both cases was about MSL + 0.34 m (Figures 6 and 8, center panel), and the simulations with higher tide (MSL + 0.68 m and MSL + 1.02 m) are included here to compare the modeled and observed effects of variable water depth.

The model starts from rest, and to avoid spin-up effects, model results are based on the last 2-hrs of 4-hr long simulations [*Yu and Slinn*, 2003]. To facilitate comparison with drifter observations, the model was extended to include Lagrangian particle tracking. Particles (10^4) were uniformly distributed in the model domain at $t = 0$, and advected by bi-linear interpolation of the nearest four Eulerian velocities and Adams-Bashford time-stepping (time step 0.1 s). After the 2-hr model spin-up, drifter releases were simulated by tracking particles selected for their proximity to the location of the actual drifter release locations (Case 1, Figure 3a, (x,y)=(90,-150); Case 2, Figure 3b, (x,y)=(110,-220) and (110,-180)). At 10 min intervals, for 50 min, the closest ten particles were selected and tracked for 40 min. Thus, 60 drifter releases spanning a 1.5 hr period were simulated for each deployment location (Case 1 - 60 total, Case 2 - 120 total). The location of simulated drifter releases is shifted seaward 20 m from the shoreline for each depth increment above MSL, thus maintaining a fixed position relative to the bathymetric inhomogeneities. Simulated and observed drifter trajectories are analyzed similarly, allowing comparison of observed (Figures 6 and 8), and simulated (Figures 12 and 14) maps of the average drifter velocities.

To isolate and examine the effects of varying bathymetry and tide level on the model flow field, values of adjustable parameters in the circulation (e.g. bottom friction) and wave transformation models were held constant. Wave conditions (H_0, T, and Θ) were also held constant (Case 1: 0.8 m, 9 s, 0^o; Case 2: 0.5 m, 7 s, 0^o). On alongshore homogenous bathymetry, the model flow vanishes with normally incident waves, so the circulations observed here result solely from alongshore bathymetric inhomogenities. The effect of bathymetric irregularities on the vorticity and velocity fields are localized (cf. *Yu and Slinn* 2003), and model results are

shown for the ≈ 300 m-long region near the domain center. To facilitate model-data Lagrangian comparisons, Case 1 drifter simulations are shown in order of decreasing depth (Figures 12).

3.1. Model-data comparsion : Case 1

Case 1 model and observation comparisons are subtle, and the Eulerian velocity and vorticity fields are presented separately to facilitate discussion. Model **u** (Figure 11a, left to right) vary only slightly as depth is increased between the MSL and MSL + 0.34 m bathymetries. This is roughly equivalent to the water level change between Figures 6a and 6d, in which flow was observed to change (as depth decreased) from a well-developed rip current (Figure 6a), ≈ MSL + 0.34 m) to a strong southward-directed alongshore current (Figure 6d), ≈ MSL). However, **u** does increase in the MSL + 0.34 m case at the same location relative to the bathymetry (see arrow, about 130,-220) as in Case 1 drifter observations (cf. Figure 4). In the next two cases (MSL + 0.68 m and MSL + 1.02 m), this trend continues, with offshore **u** in the last (highest tide level) case more than doubling relative to the lowest tide level. Note also, that as the **u** peak strengthens, it moves closer to the surfzone seaward edge.

A dominant feature in all four cases of the model alongshore velocities (**v**) (Figure 11b, left to right) was a strong, narrow, southward-flowing alongshore current. Drifter trajectories and velocities observed during Case 1 (Figures 5 and 6 c,d) were consistent with entrainment in a similar flow. A more subtle feature of the flow varies significantly with increasing water depth (see arrows). A northward-directed flow, between about alongshore (-350:-150) and cross-shore (120:180) in the MSL case, decreases with each increase in depth, finally becoming almost nonexistent.

The Case 1 vorticity simulations suggest strongly that the eddy is bathymetrically controlled, as it located over a bend in the bottom contours at all four tide levels (see arrows), as in the

drifter data (Figure 5).) All other drifter-delineated surfzone eddies we observed have similarly maintained position, and when bathymetry was available, were located over a bathymetric depression (*Schmidt* 2003; *Schmidt et al.* 2003, and additional observations).

As previously noted, Case 1 simulated drifter releases (Figures 12a-d) are presented in order of decreasing water depth to facilitate comparison with the observations (Figures 6a-d). The MSL + 1.02 m case spatial means are consistent with a narrow, seaward-directed current embedded in a more diffuse offshore flow (Figure 12a). The current is slightly oblique to shore-normal, although it exits the surf zone in roughly the same location (y≈-250) as the observed shore-normal rip (Figure 6a). The velocity maxima occurs near the surfzone edge and the rip current extends seaward roughly 1.5 surfzone widths from the shoreline (x = -40, not shown). In Figure 12b (MSL + 0.68 m), the narrow seaward current has weakened, its orientation is more shore-parallel, and the location at which it exits the surf is less distinct. The diffuse offshore flow is also weaker and its offshore extent is reduced. A CW re-circulation cell, so named because it straddles the surfzone edge, exhibits spatially-variable vorticity, and does not advect drifters in closed paths, begins to entrain drifters and is centered at roughly (180,-320). In subsequent water depth decrements (Figs. 12c,d; MSL + 0.34 m and MSL, respectively), the simulated drifter velocities show the offshore flow continuing to weaken. Finally, the offshore flow between alongshore (-275:225) is no longer present, while the re-circulation cell strengthens to become the dominant flow feature in the simulated drifter data. In place of the narrow offshore flow seen in Figure 12a, an onshore flow of roughly equal strength and width is present in Figure 12d, and the model drifters are advected alongshore ≈200 m from their release point. The observed drifters were also advected alongshore at lower tide levels, but were entrained in

a CCW eddy (Figure 6d) that is present in the simulations (long arrows, Figure 11c), but which did not entrain the simulated drifters.

Although with decreasing tide level the modeled and observed drifter trajectories both transition from a shore-normal path to an eddy-dominated alongshore motion (compare Figure 6 with Figure 12), the water depths are different (center panels, Figures 6 and 12).

3.2. Model-Data Comparison : Case 2

The strongest simulated Eulerian offshore flow occurs at the lowest tide levels (Figures 13a, b). Maximum velocities in both branches of the bifurcated rip occur near the surfzone edge, and both branches extend roughly 2 surfzone widths offshore (although the simulated right branch recurves shoreward). At higher tide levels the model vorticity decreases, and the branches become less distinct (Figures 13c, d). At the highest simulated tide level, the model cross-shore velocities at the surfzone edge are a factor of 2 lower than at the lowest tide level (*Schmidt* 2003).

The observed and modeled evolution of drifter velocities with rising tide are similar (compare Figure 8 with Figure 14). At low tide levels, drifters are advected seaward in the bifurcated rip current. At higher tide levels the simulated flow weakens, although in the model the south branch is the more persistent (Figure 14c) whereas the north branch persists longer in the observations (Figure 8c). As in Case 1, the simulated and observed circulation patterns evolve similarly, but the depths are generally greater in the simulation with similar circulation (center panels, Figures 8 and 14).

4. Discussion

Model velocities and vorticities are generally lower than those observed by about a factor of 2, with the exception Case 2 low tide (Figures 8a and 14a). Tuning the value of C_f could presumably bring the model velocities closer to the observations. Excepting Case 1 MSL (Figures 6d and 12d), model water depths needed to reproduce the observed flows were higher, due in part to previously discussed model domain bathymetric constraints, but possibly in part due to parameters in the breaking wave model used to estimate wave forcing. As previously noted, C_f and other adjustable model parameters were not altered in this series of experiments.

Differences in Case 1 and Case 2 flows result from differences in bathymetry. In MSL simulations with reversed wave forcing (e.g. Case 1 bathymetry and Case 2 wave conditions, and vice-versa, not shown), the bifurcated offshore flow stayed with the Case 2 bathmetry, and (southerly) alongshore flow stayed with the Case 1 bathymetry. That is, the model is more sensitive to differences in Case 1 and Case 2 bathymetries, than to different wave forcing.

5. Case 1 Model Momentum Balances

Figures 15a-d show the spatial distribution of the first 4 terms in (2), with advective terms grouped. Though non-uniform in both alongshore and cross-shore directions, the balance is generally between wave-forcing (τ_y) and the sum of the pressure gradient (dp/dy), advection, and friction terms, with biharmonic dissipation insignificant at O($\pm 10^{-7}$) (not shown, compare with residual, O($\pm 10^{-5}$)). This contrasts with the case of obliquely incident waves on alongshore homogeneous bathymetry, where wave forcing is balanced primarily by friction (cf. *Ruessink et al.* 2001).

The cross-shore balance (3) is dominated by wave forcing (τ_x) and pressure gradient (dp/dx), as in recent laboratory and numerical models (i.e., *Haller et al* 2002 and *Dean and Brown*

1995). These terms are the largest of either alongshore or cross-shore balance (O($\pm$ 2 x 10^{-2}) (Figures 16a,b). A more detailed description of the cross-shore momentum balance is made by comparing the relatively small sum of the dp/dx and τ_x terms (Figure 16c), with the friction and advective terms (Figs. 16d, e). At this level, the balance is clearest between dp/dx+τ_x and advection, with friction relatively unimportant. This same relationship can be seen with careful examination of *Haller et al* 2002 (Figures 11 and 12), and *Dean and Brown* 1995 (Figure 16).

In the Case 1 MSL simulation, the only strong cross-shore flow was associated with the CCW eddy centered at (x,y)=(120,-380), in rough agreement with observations. The dp/dx+τ_x term in the region between alongshore (-170:-250) in the MSL case is offshore-directed, though weak, at roughly cross-shore (70:120) (see arrow, Figure 16c). In subsequent increasing water levels, this feature strengthens and moves closer to the seaward surfzone edge (x$\approx$ 200) (Figure 17). The overall balance in this region (alongshore (-170:-250)) is still clearly between dp/dx+τ_x and advection, especially as **u** increases.

6. Conclusions

Surfzone currents on alongshore variable bathymetry were observed with recently developed GPS-tracked drifters. Trajectories of ten drifters repeatedly released near an irregularly shaped bar-trough bathymetric feature in 1 to 2 m water depth sometimes define rip currents and surfzone eddies, flow features that have been difficult to resolve with fixed instruments. Rip currents were strongest at the surfzone edge and extended offshore about 2 surfzone widths. A bifurcated rip current was observed to be capable of exchanging surfzone water over a 600 m alongshore span in about an hour. A 40 m diameter surfzone eddy was observed over a bathymetric depression, and persisted for at least 1 hr.

Two days, one each from July 2001 and July 2002 (denoted Case 1 and Case 2), were selected for detailed analysis. The drifter-deliniated surfzone circulation evolved as the tide level changed during each 4-6 hr long deployment period. As the tide dropped during Case 1, a shore-normal rip current present for the first 2 hr evolved in a shore-parallel flow. As the tide rose during Case 2, the well-developed, bifurcated rip current observed for 2 hr was replaced by a weak, amorphous circulation.

Circulations and model drifter trajectories, qualitatively similar to the observations, are predicted by the time-dependent, nonlinear shallow water equations forced by breaking waves and using the measured bathymetry, although observed and modeled velocities differed by roughly a factor of 2. The radically different circulations observed in 2001 and 2002 are attributed to relatively small differences in surfzone bathymetry. The modulations in flow observed on two particular days during approximately 0.5 m changes in tide level were also successfully simulated, however, the simulated water levels were required to vary by about 1 m.

The cross-shore momentum balance was dominated by wave-forcing and pressure gradient terms of about equal magnitude and opposite sign, as seen in previous studies. In the vicinity of a simulated rip current, the residual of the forcing and pressure gradient was balanced primarily with advection terms. The alongshore momentum balance was complicated, with about equal contributions from wave forcing, alongshore pressure gradients, friction, and advective terms.

Acknowledgments

Funding was provided in part by the National Sea Grant College Program, National Oceanic and Atmospheric Administration, U.S. Department of Commerce, under grant NA06RG0142, project R/CZ-166 through the California Sea Grant College Program, and by the California State Resources Agency. The views expressed herein are those of the authors and do not necessarily reflect the views of NOAA or any of its sub-agencies. The U.S. Government is authorized to reproduce and distribute for governmental purposes. The Office of Naval Research and the National Science Foundation also provided funding.

Technical support from the Center for Coastal Studies and the Scripps Institution of Oceanography Hydraulics Laboratory is gratefully acknowledged. In particular, Brian Woodward, Kimball Millikan, Dennis Darnell, Bill Boyd, Kent Smith, Jerome Wanetick, Charly Coughran, Fred Wright, John Lyons and David Aglietti were instrumental in the fabrication, testing, and data gathering portions of this work. Rob Holman (Oregon State University) and the Coastal Imaging Laboratory (CIL) staff furnished rectified video images of the study site. Bill O'Reilly (University of California, San Diego) and the staff of the Coastal Data information Program (CDIP) supplied offshore wave data. Lt. Brant Bass and the San Diego Lifeguard Department provided valuable support during field operations.

References

Allen,J. S., P. A. Newberger, and R. A. Holman, 1996: Nonlinear shear instabilities of alongshore currents on plane beaches, *J. Fluid Mech.* **310**, 181 - 213.

Chen, Q., R. A. Dalrymple, J. T. Kirby, A. B. Kennedy, and M. C. Haller, 1999: Boussinesq modeling of a rip current system. *J. Geophys. Res.,* **104**, 20,617-20,637.

Dean, W. R., and C. A. Brown, 1995: A modeling investigation of the breaking wave roller with applications to cross-shore currents, *J. Geophys. Res.,* **100**, 24,873 - 24,883.

Dronen, N., H. Karunarathna, J. Fredsoe, B. M. Sumer, and R. Deigaard, 1999: The circulation over a longshore bar with rip channels. *Proc. Coastal Sediments '99*, Hauppauge, NY, Amer. Soc. Mech. Engr. 576-587.

Haas, K., and I.A. Svendsen, 2002: Laboratory measurements of the vertical structure of rip currents. *J. Geophys. Res.,* **107**, doi:10.1029/2001JC000911.

Haas, K., I. A. Svendsen, M. Haller, and Q. Zhao, 2003: Quasi-three-dimensional modeling of rip current systems. *J. Geophys. Res.,* **107**, doi:10.1029/2002JC001355.

Haller, M., R. Dalrymple, and I. Svendsen, 2002: Experimental study of nearshore dynamics on a barred beach with rip channels. *J. Geophys. Res.,* **108**, doi:10.1029/2001JC000955.

Hino, M., 1974: Theory on formation of rip-current and cuspidal coast, *Proc. 14th Conf. Coastal Eng.*, 901-919.

Hite, M. P. 1925: The "Undertow", *Science*, **62**, 32-33, 1925.

Holland, K. T., R. A. Holman, T. C. Lippmann, J. Stanley, and N. Plant, 1997: Practical use of video imagery in nearshore oceanographic field studies, *J. Oceanic Eng.* **22**, 81-92.

Johnson, D. and C. Pattriaratchi, 2004: Transient rip currents and nearshore circulation on a swell dominated beach. *J. Geophys. Res.,* **109**, doi:10.1029/2003JC001798.

Longuet-Higgins, M. S., 1970: Longshore currents generated by obliquely incident seawaves, 1. *J. Geophys. Res.,* **75,** 6790-6801.

Putnam, J. P., W. H. Munk, and M. A. Traylor, 1949: The prediction of longshore currents, *Transactions, American Geophysical Union* **30**, 337-345.

Ranasinghe, R., G. Symonds, K. Black, and R. Holman, 2000: Processes governing rip spacing, persistence, and strength in a swell dominated microtidal environment, *Coastal Eng. 2000* **1**, 454-467.

Ruessink B. G., J. R. Miles, F. Feddersen, R. T. Guza, and S. Elgar, 2001: Modeling the alongshore current on barred beaches, *J.* Geophysical Research, 106, 22,451-22,463.

Schmidt, W. E., B. T. Woodward, K. S. Millikan, R. T. Guza, B. Raubenheimer and S. Elgar, 2003: A GPS-tracked surfzone drifter, *J. Atmos. and Ocean. Tech.*, **20**, 1069-1075.

Schmidt, W. E., 2003: Lagrangian observations of surfzone currents. Ph.D. dissertation, 105 pp., Univ. Calif. San Diego..

Shepard, F. P., K. O. Emery, and E. C. La Fond, 1941: Rip currents: a process of geological importance. *J. Geol.*, **49,** 337-369.

Shepard, F. P. and D. L. Inman, 1950: Nearshore water circulation related to bottom topography and wave refraction. *Trans. Amer. Geophys. Union* **31,** 196-212.

Slinn, D. N., J. S. Allen, P. A. Newberger, and R. A. Holman, 1998: Nonlinear shear instabilities of alongshore currents over barred beaches, *J. Geophys. Res.,* **103**, 18,357 - 18,379.

Slinn, D. N., J. S. Allen, and R. A. Holman, 2000: Alongshore currents over variable beach topography, *J. Geophys. Res.,* **105**, 16,971 - 16,998.

Sonu, C. J., 1972: Field observations of nearshore circulation and meandering currents. *J. Geophys. Res.,* **77,** 3232-3247.

Thorton, E. B., and R. T. Guza, 1986: Transformation of wave height distribution. *J. Geophys. Res.,* **88**, 5929 - 5938.

Wright, D. W., and K. R. Thompson, 1983: Time-averaged forms of the nonlinear stress law. *J. Phys. Oceanogr.,* **13**, 341-346.

Yu, J., and D. N. Slinn, 2003: Effects of wave-current interaction on rip currents. *J. Geophys. Res.,* **108**, doi:10.1029/2001JC001105.

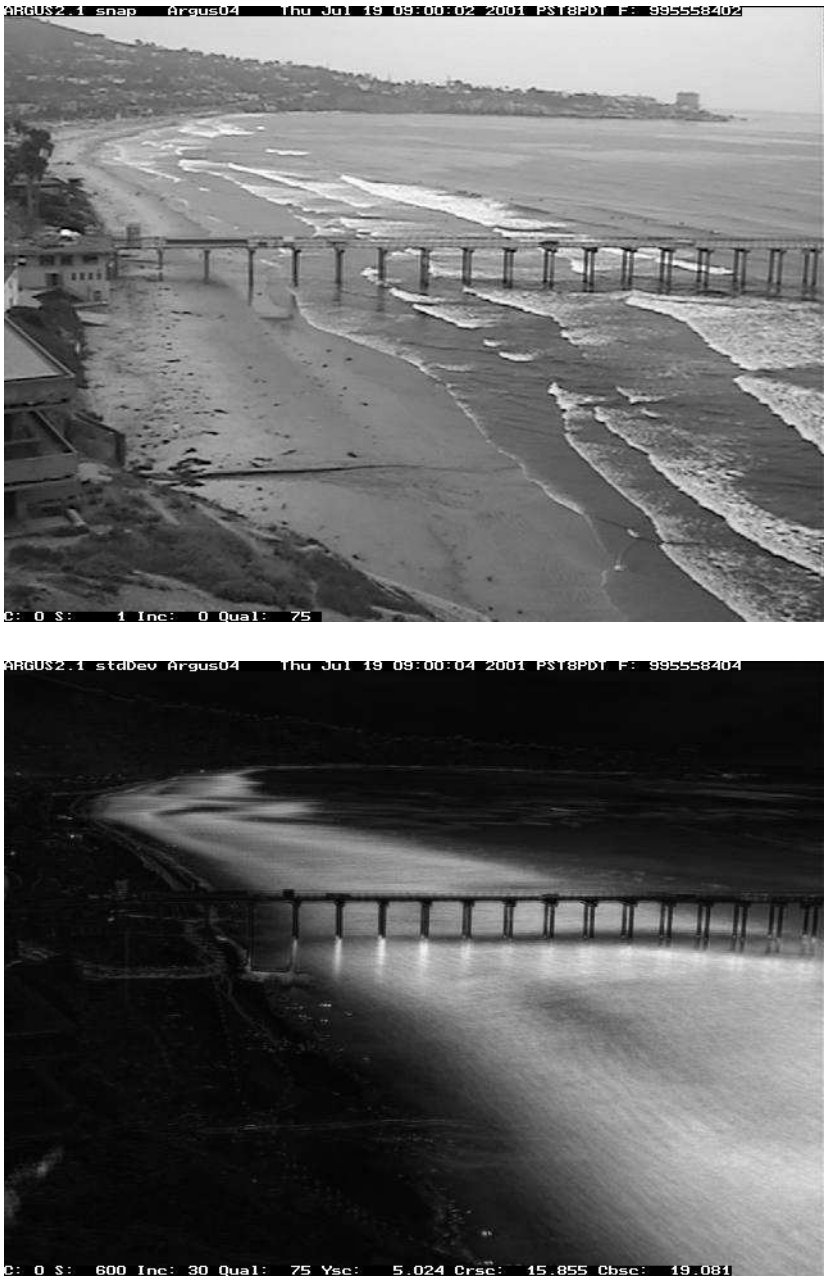

Figure 1. Images from a CIL Argus camera, looking south towards the study site located 400 m south of SIO pier, on 19 July 2001 (later referred to as Case 1). (top) Snapshot. (bottom) Time lapse pixel variance, where bright regions are areas of persistent wave breaking, dark regions are areas of relatively quiescent water or land (R. Holman, personal communication).

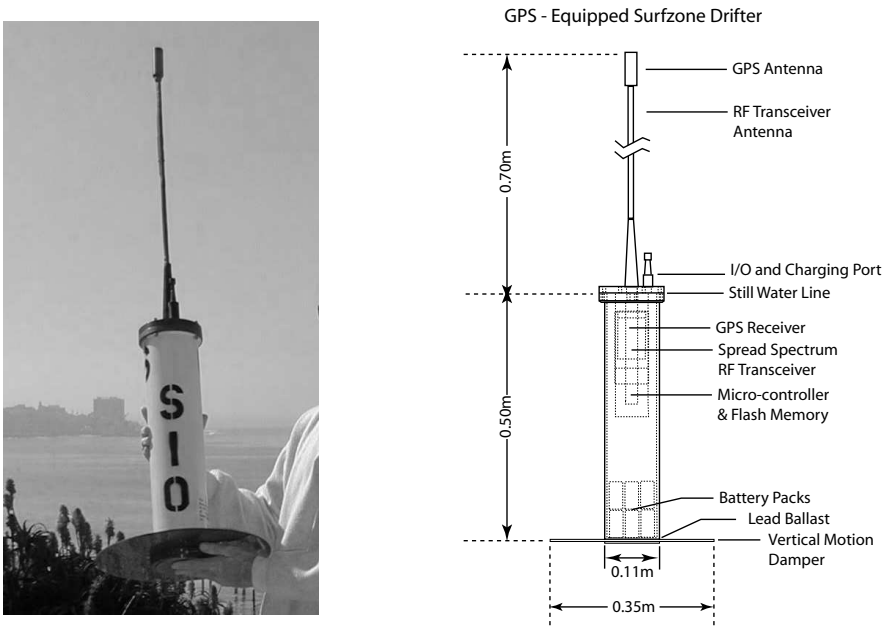

Figure 2. Photograph and schematic of the surfzone drifter. Surface piercing antennae for receiving GPS signals and for radio-frequency (RF) communication with shore are molded permanently to the drifter top cap. A 6-pin port, also integral to the top cap, permits programming and data downloading (I/O), and battery charging without opening the drifter package.

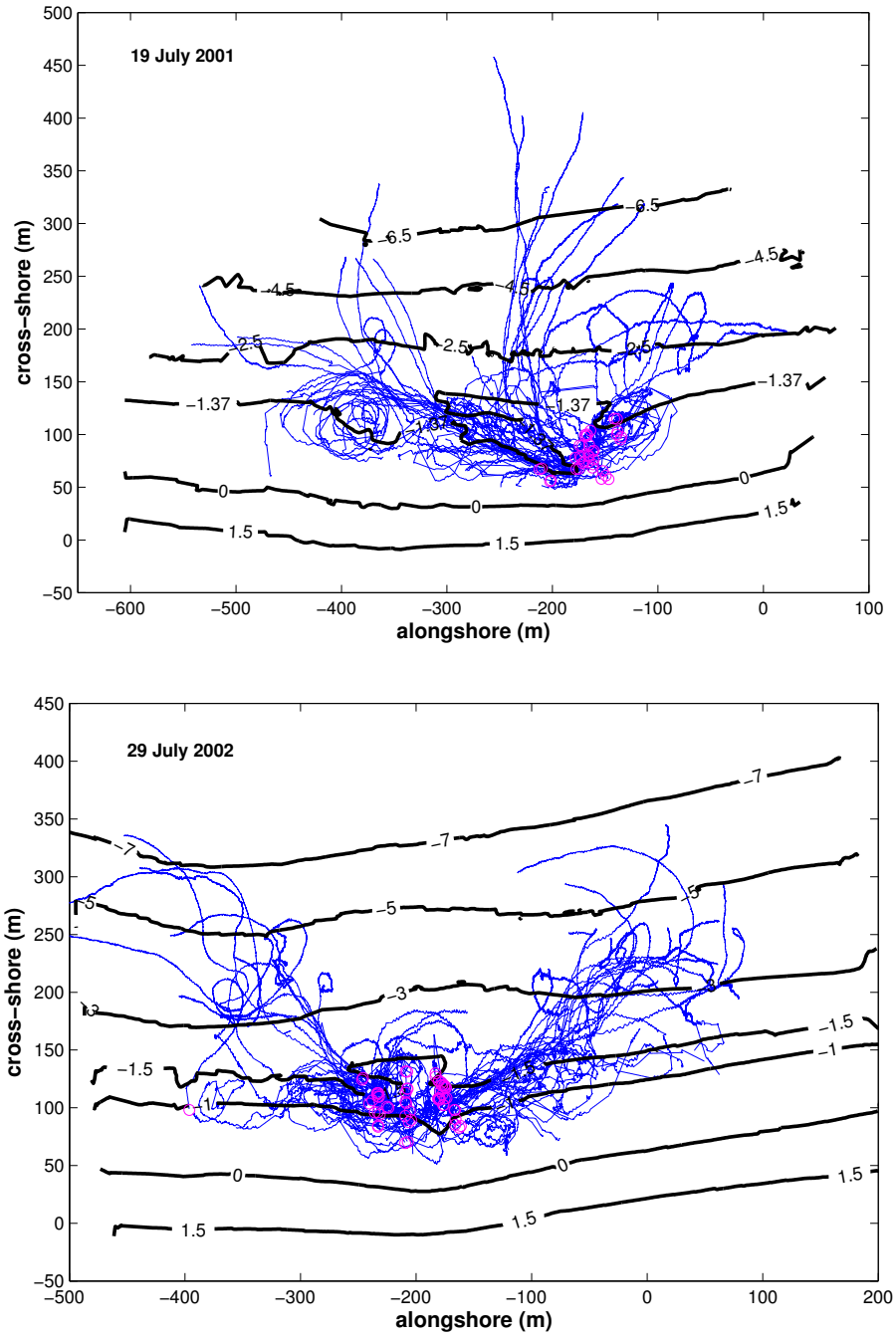

Figure 3. (top) 19 July 2001, UTC 16:24-21:35 (Case 1) and (bottom) 29 July 2002, UTC 14:20-18:48 (Case 2) drifter deployments. Thin blue curves are drifter trajectories. Thick black curves are depth contours. Magenta circles are deployment locations.

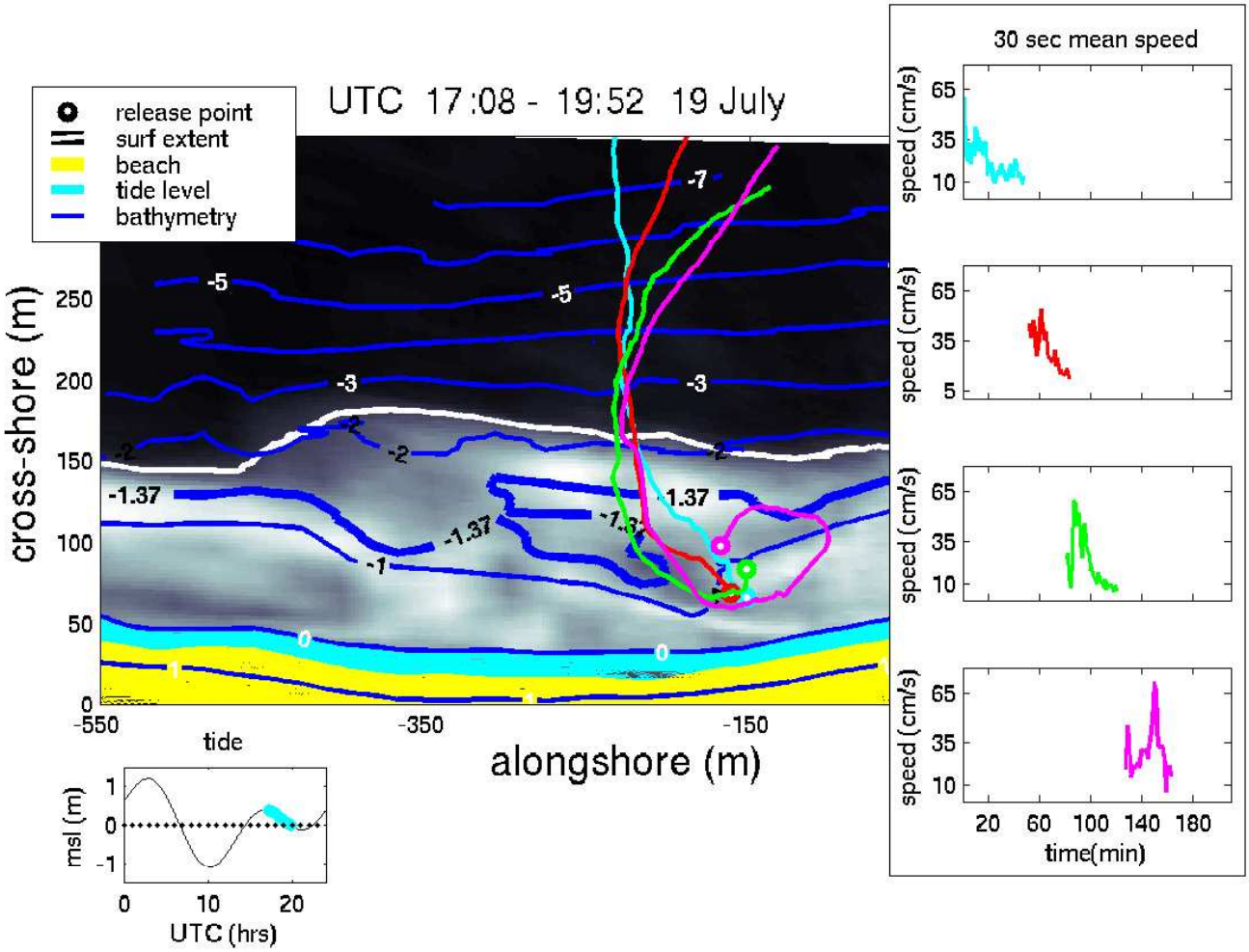

Figure 4. CIL time-lapse image from Case 1 (cf. Figure 1) rectified and overlain with bathymetry (dark blue curves are depth contours (m) relative to MSL). Selected drifter trajectories (colored curves) are consistent with entrainment in a roughly shore normal rip current. Partially-filled colored circles denote drifter release locations. Yellow region is above tide level (i.e., the subaerial beach). Light blue region shows the range of the mean waterline during the $\approx$ 3-hr period. Lower left inset panel indicates tide level for the UTC day (black curve), and for the 3-hr period (light blue curve). Inset panel at right shows 30 sec mean speeds versus time since the first deployment shown (17:08). Cross-shore drifter velocities are maximum near the seward edge of the surfzone (bold white curve).

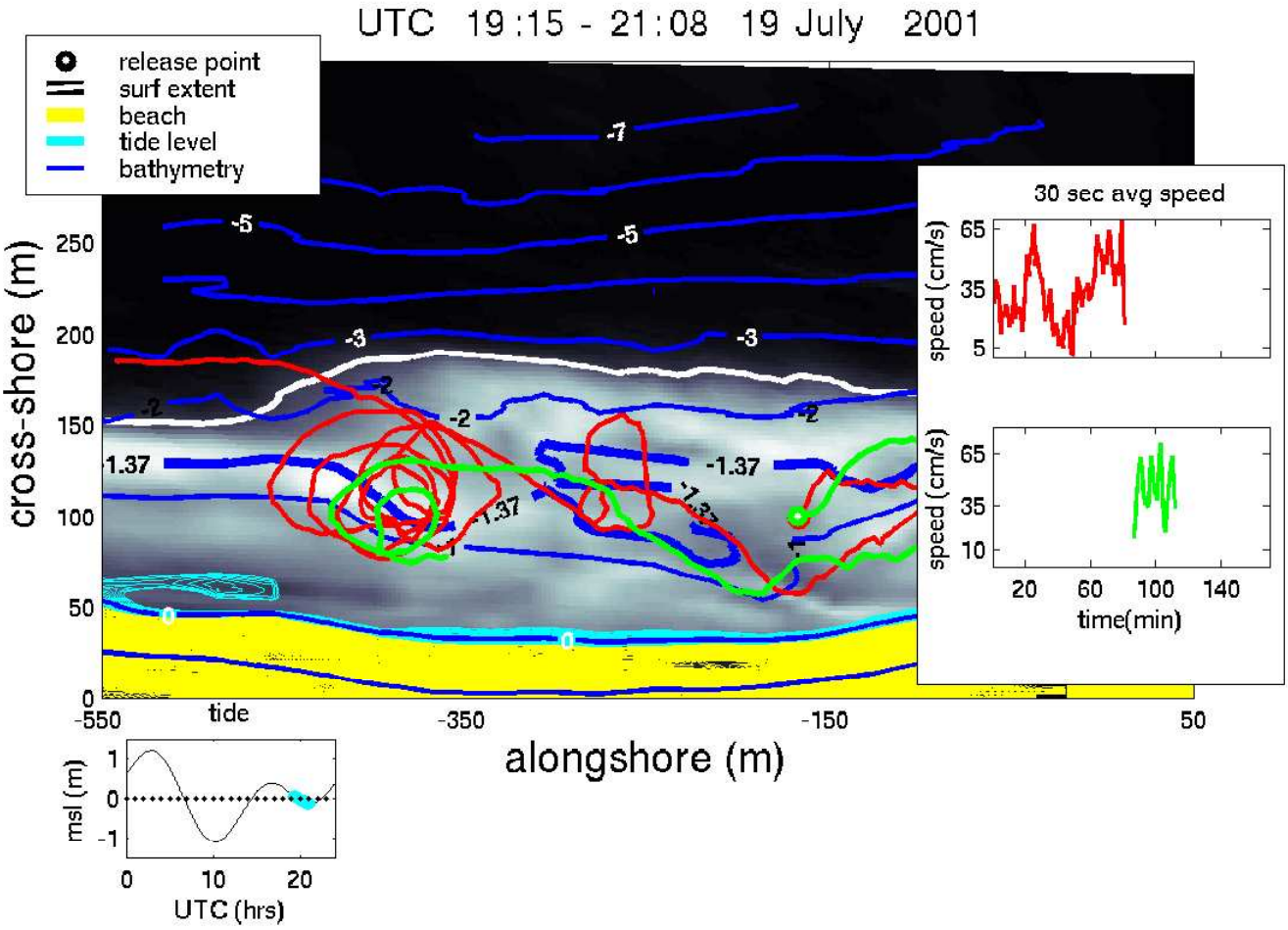

Figure 5. Selected drifter trajectories (red and green curves) for Case 1 (19 July 2001) are consistent with entrainment in a counter-clockwise eddy centered near (cross-shore, alongshore) coordinate (110,-375). The format is similar to Figure 4.

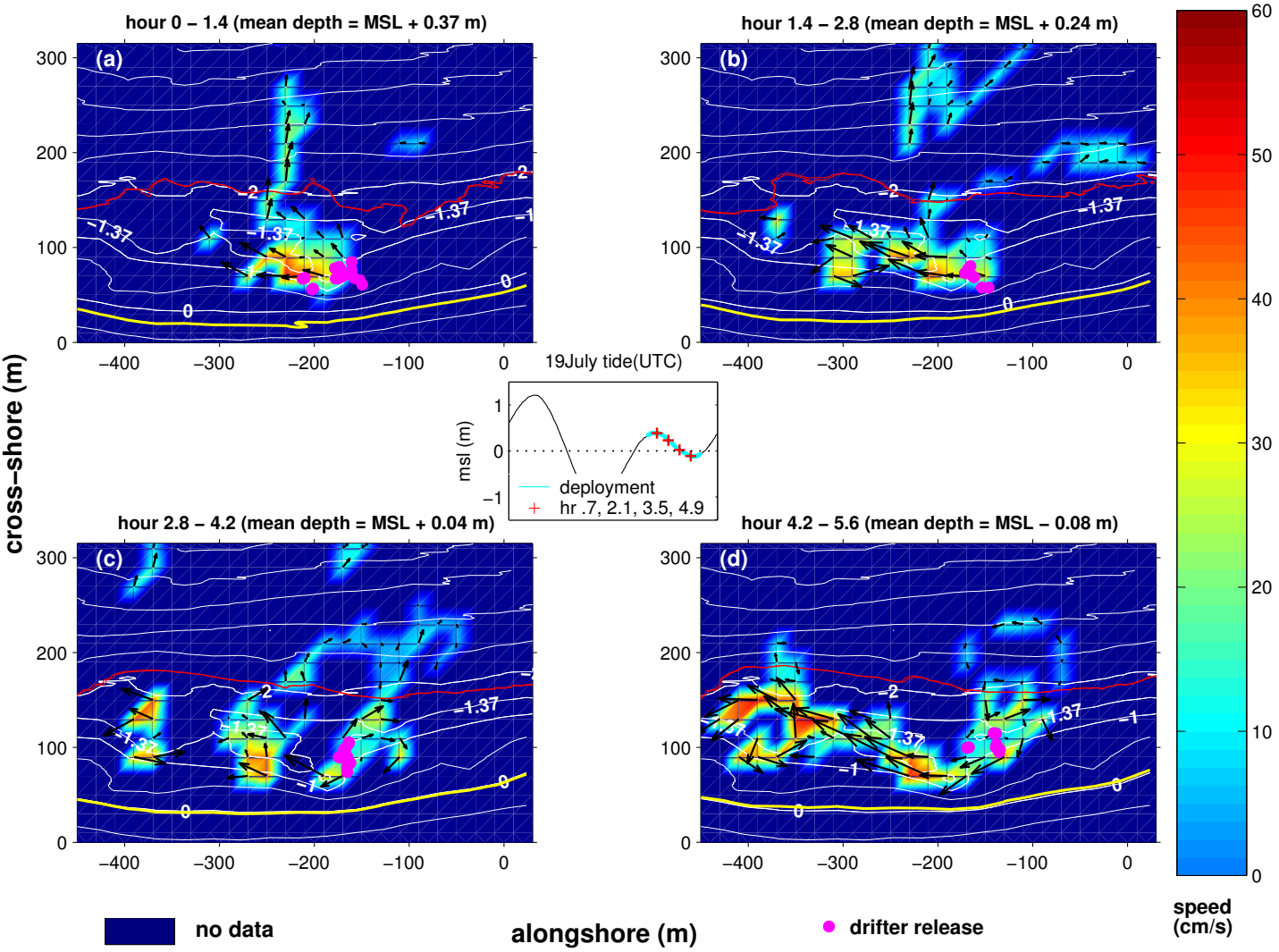

Figure 6. Observed Case 1 (19 July 2001) spatially (20 m by 20 m bins) and temporally (30 s) averaged drifter velocities. There are a minimum of 5 means in each bin. Colors denote velocity magnitude, and arrows indicate velocity direction and relative magnitude. Dark blue regions were not sampled by the drifters. Thin white curves are bathymetric contours (relative to MSL), red curve is surfzone extent, and yellow curve is the mean waterline. Magenta circles show locations of drifter releases. Time periods shown are (a) 0 to 1.4, (b) 1.4 to 2.8, (c) 2.8 to 4.2, and (d) 4.2 to 5.6 hrs after the UTC 16:24 start time. Center panel shows tide level for entire UTC day (thin black curve), and mean tide level of (a) - (d) (red plusses).

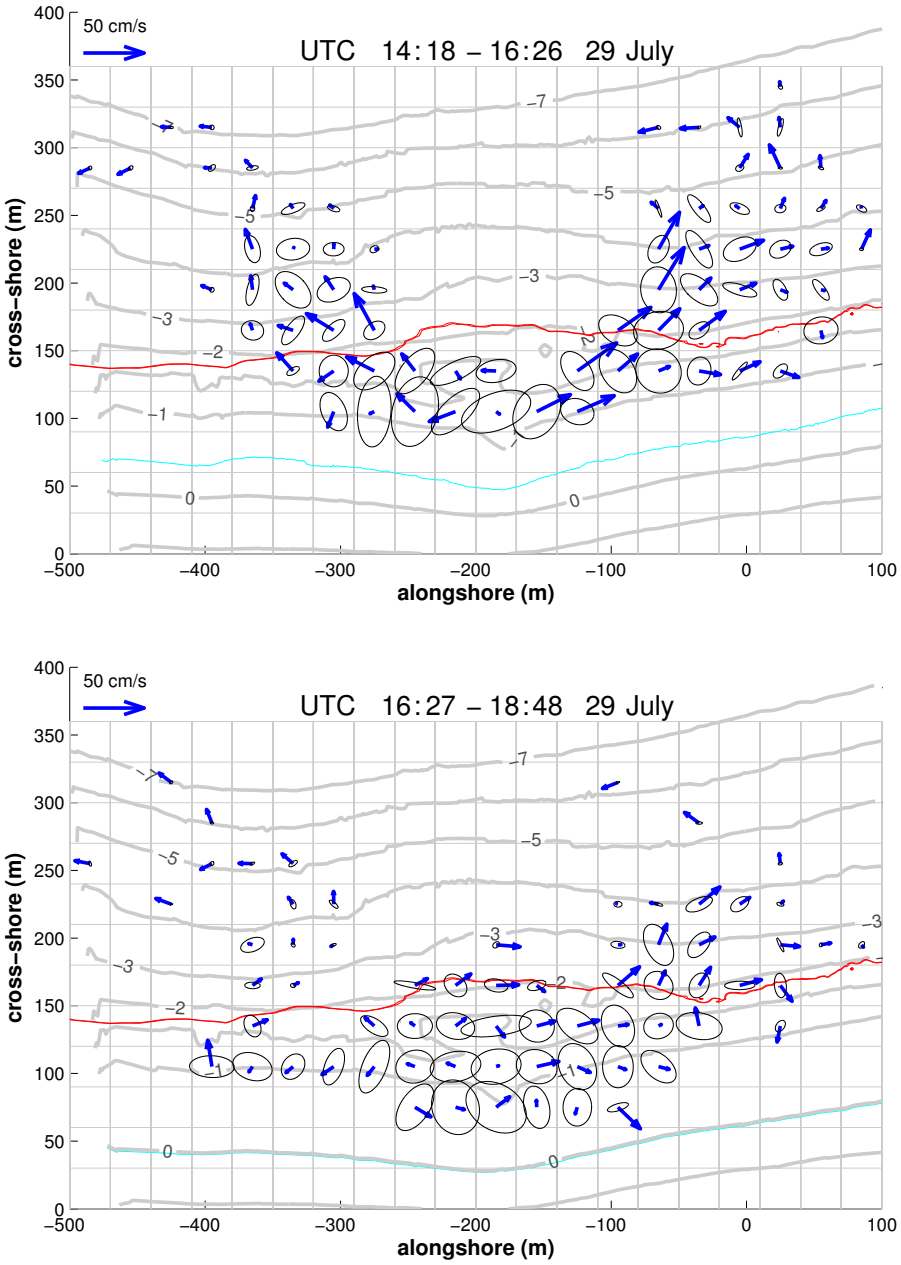

Figure 7. Spatially (30 m by 30 m bins, gray boxes) and temporally (30 s) averaged mean drifter velocities and variance ellipsi for Case 2 , 29 July 2002. (top) UTC 14:16-16:26. (bottom) UTC 16:27-18:48. There are a minimum of 5 means per bin. Arrows indicate mean velocity direction and magnitude. Thin gray curves are bathymetric contours (relative to MSL), red curve is surfzone extent, and light blue curve is the mean waterline. Drifter release locations are centered around (x, y)= (100,-200) (cf. Figure 3b). Some drifters from the first half of the deployment (top) remained in the water during the last half (bottom).

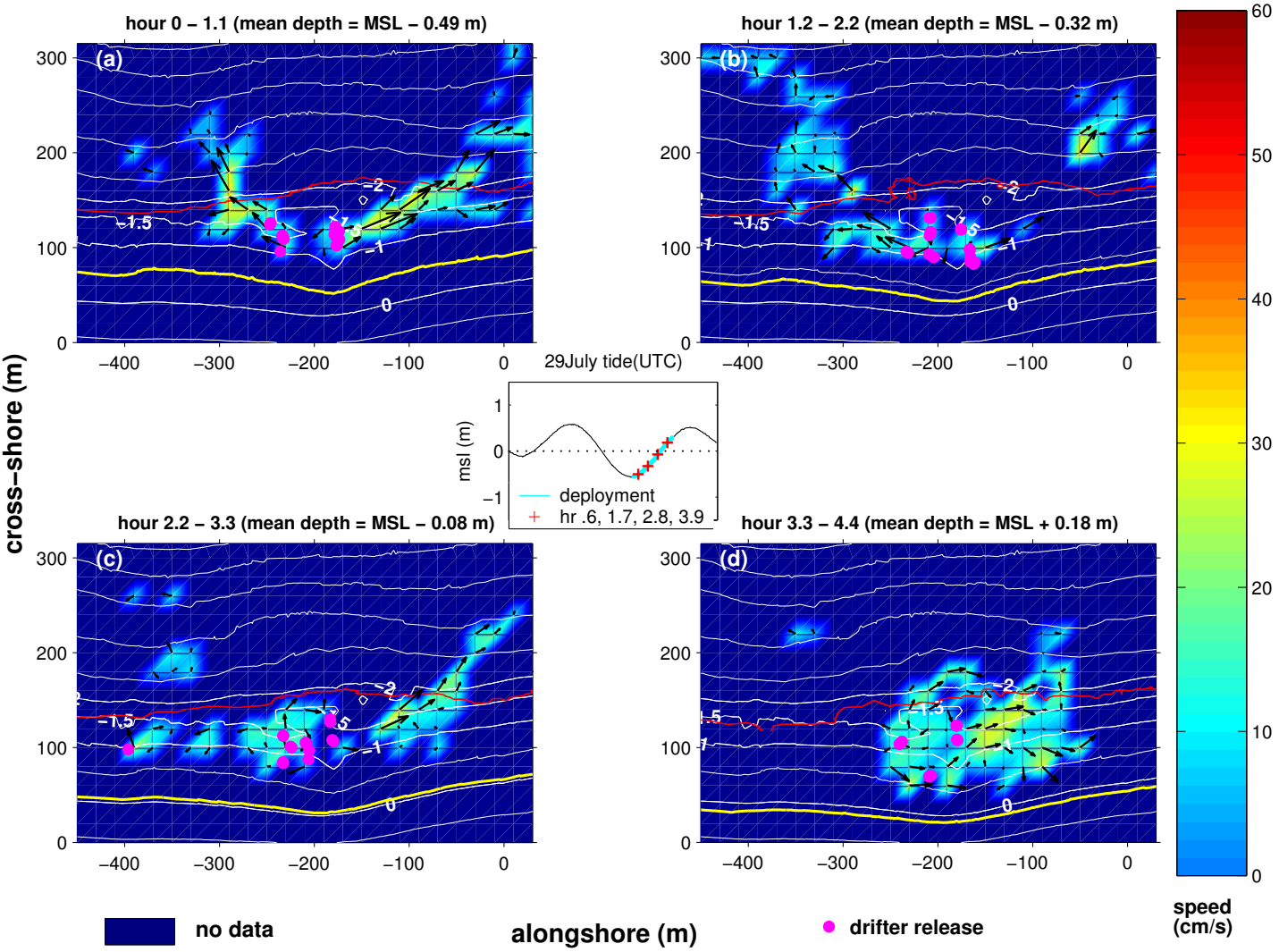

Figure 8. Observed Case 2 (19 July 2002) averaged drifter velocities. See Figure 6 format. Time periods shown are (a) 0 to 1.1, (b) 1.1 to 2.2, (c) 2.2 to 3.3, and (d) 3.3 to 4.4 hrs after the UTC 14:18 start time.

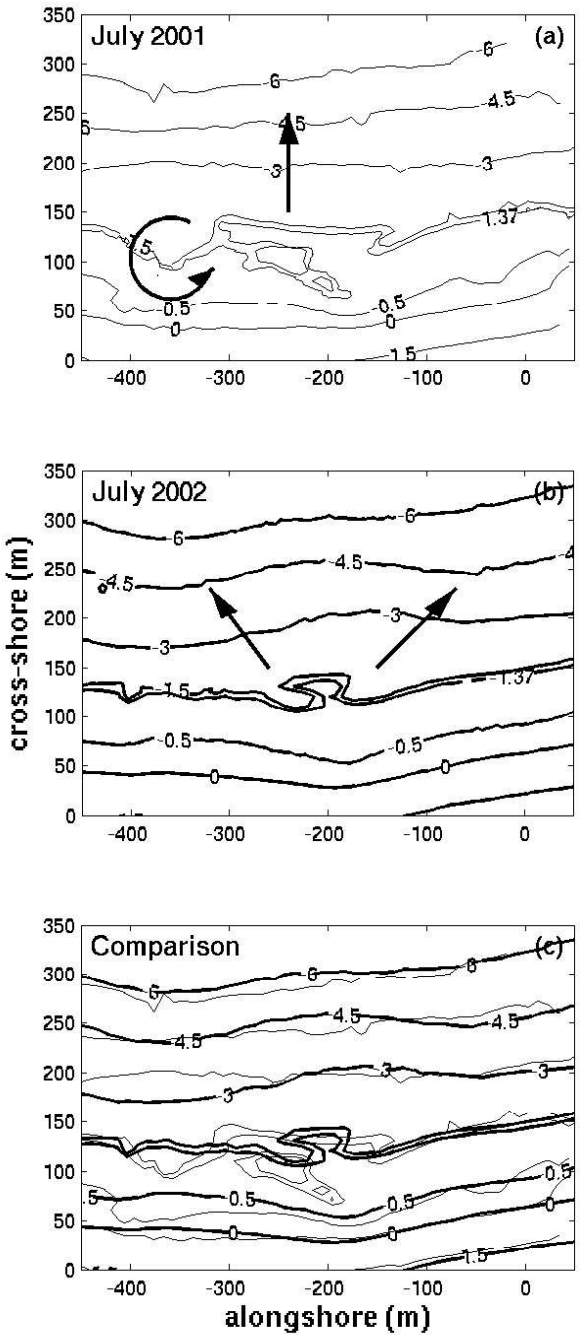

Figure 9. (a) Case 1 bathymetry (thin black curves, relative to MSL) and location of observed shore-normal rip (straight black arrow) and surfzone eddy (curved black arrow) and (b) Case 2 bathymetry (thick black curves) and location of bifurcated rip branches (black arrows). (c) Thin and thick black curves are Cases 1 and 2 bathymetric contours, respectively.

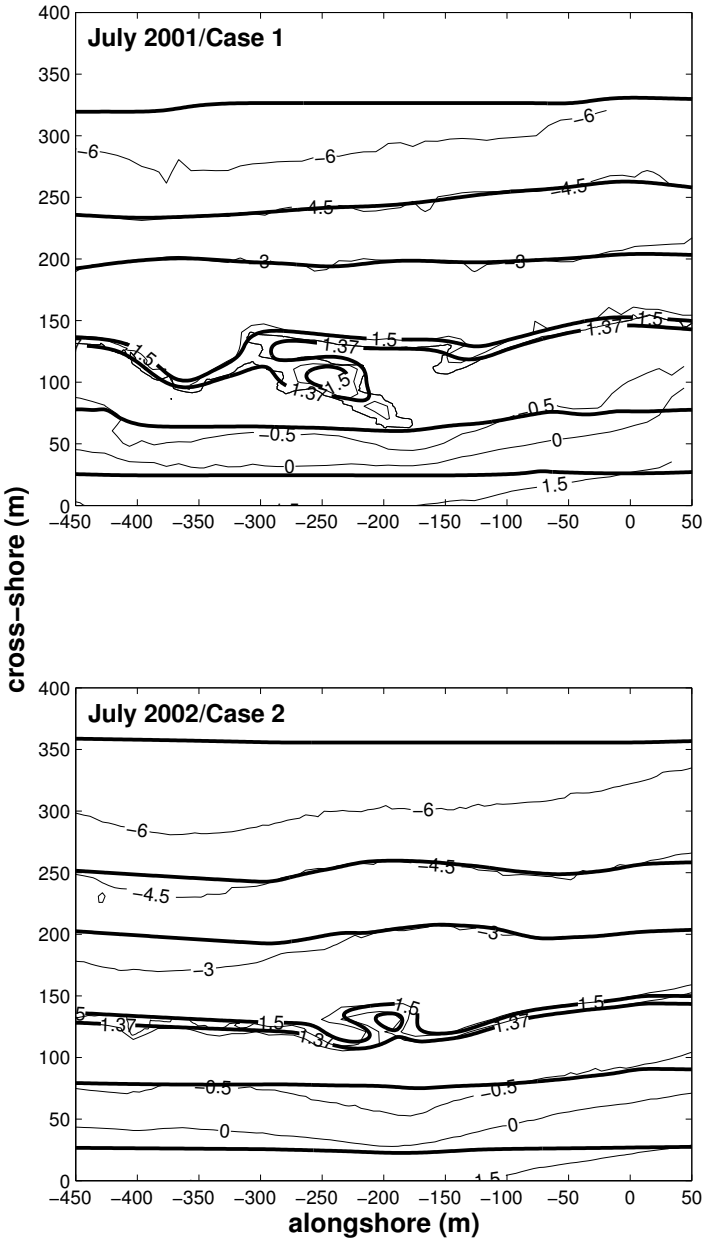

Figure 10. (top) Case 1 observed bathymetry (thin black curves, relative to MSL) and Case 1 model MSL bathymetry (thick black curves). (bottom) Case 2 observed bathymetry (thin black curves, relative to MSL) and Case 2 model MSL bathymetry (thick black curves).

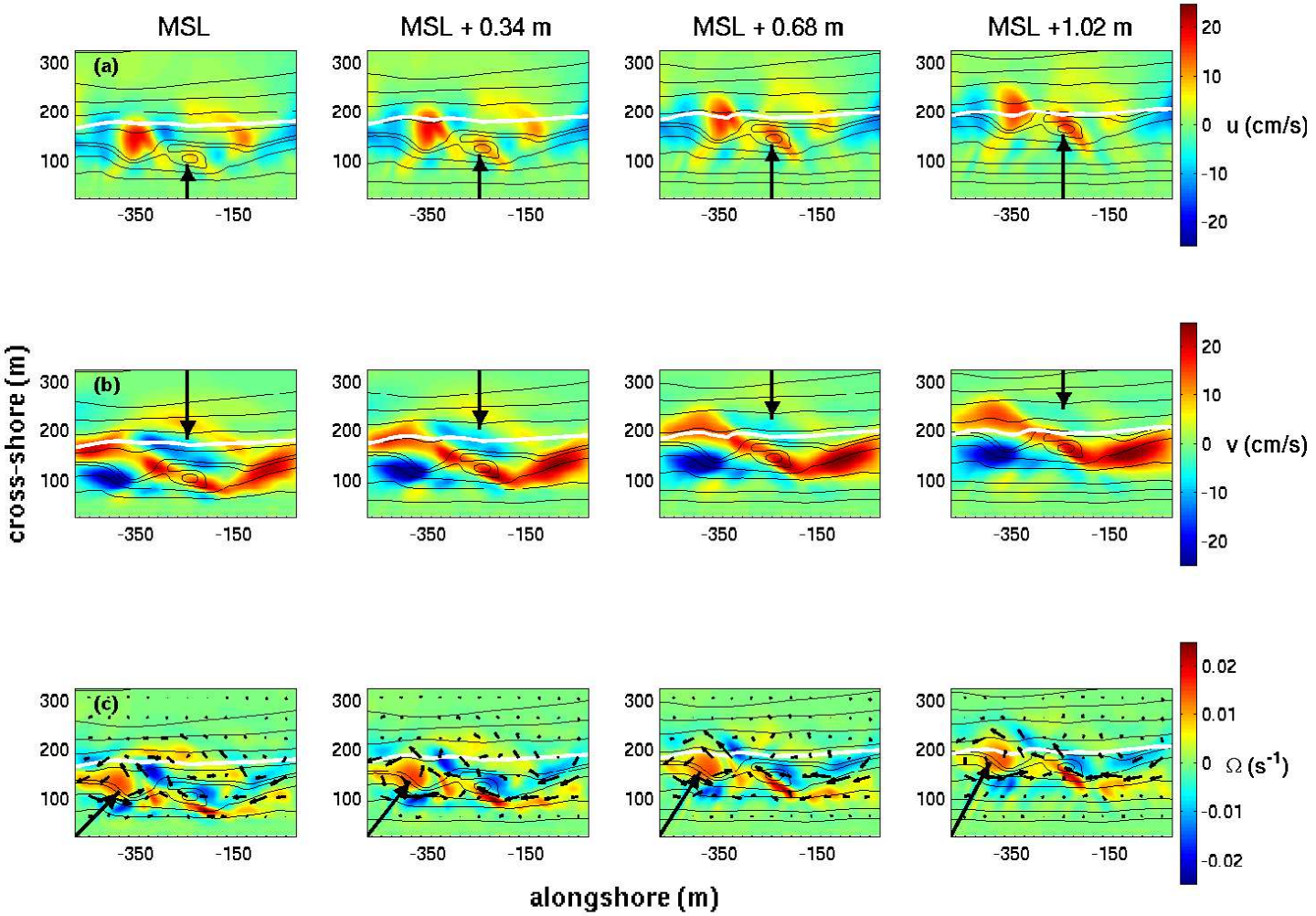

Figure 11. Case 1 time mean (2 hr) model flow parameters at tide levels of MSL, MSL + 0.34 m, MSL + 0.68 m, MSL + 1.02 m. (a, left to right) Cross-shore velocity (red - offshore, blue - onshore). (b, left to right) Alongshore velocity (red - southward (left)), blue - northward (right)). (c, left to right) Vorticity (red - CCW, blue - CW) and velocity (arrows indicate direction and relative magnitude). Black curves are bathymetric contours. White curve is model surf extent. Large arrows indicate flow features discussed in text.

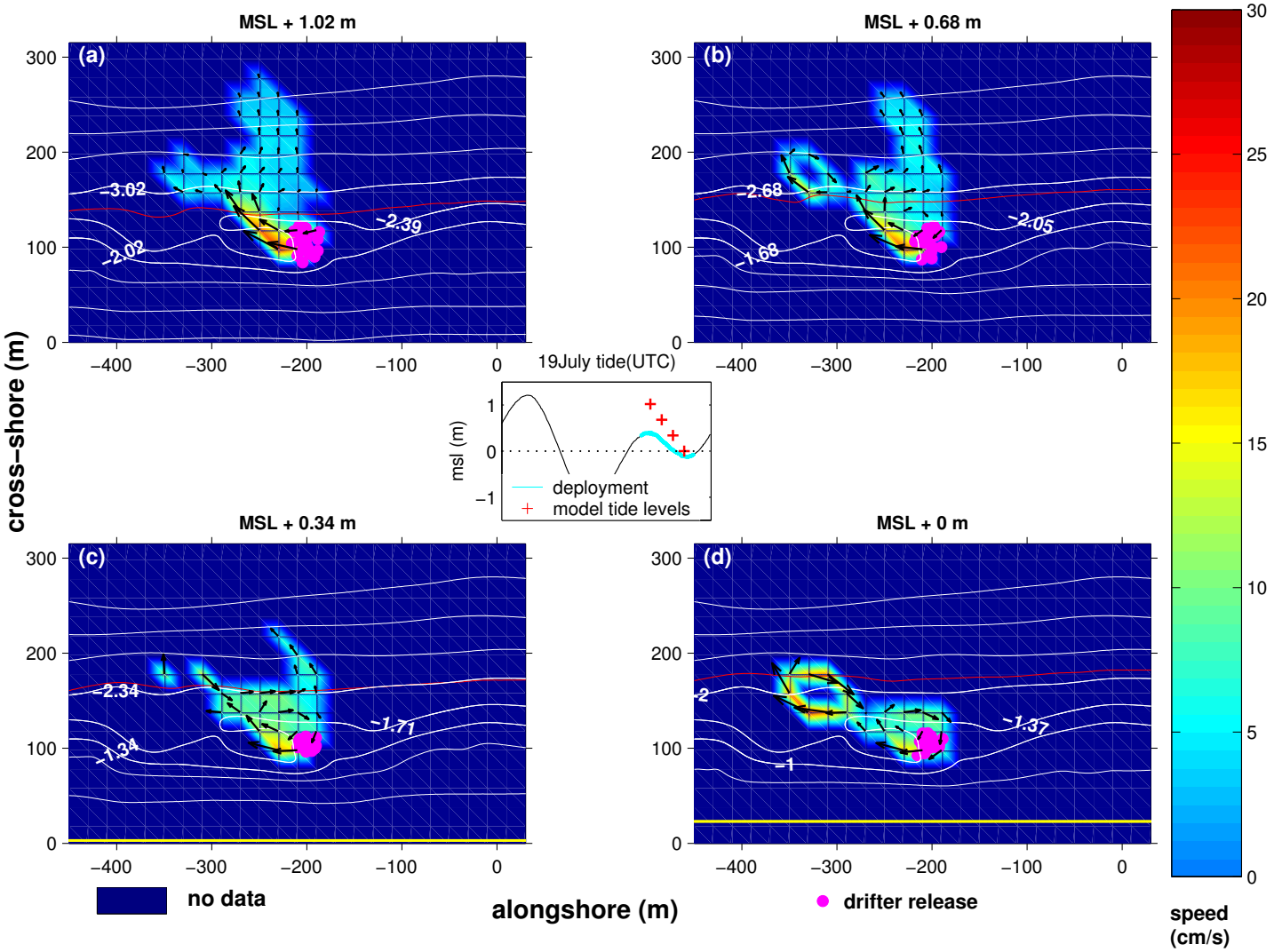

Figure 12. Simulated Case 1 spatially and temporally averaged drifter velocities. See Figure 6 format. Tide levels are (a) MSL + 1.02 m, (b) MSL + 0.68 m, (c) MSL + 0.34 m, and (d) MSL. Center panel shows tide level for UTC 19 July 2001 (thin black curve), tide level during Case 1 observations (cyan curve), and discrete tide levels of the present Case 1 simulations (red asterisks).

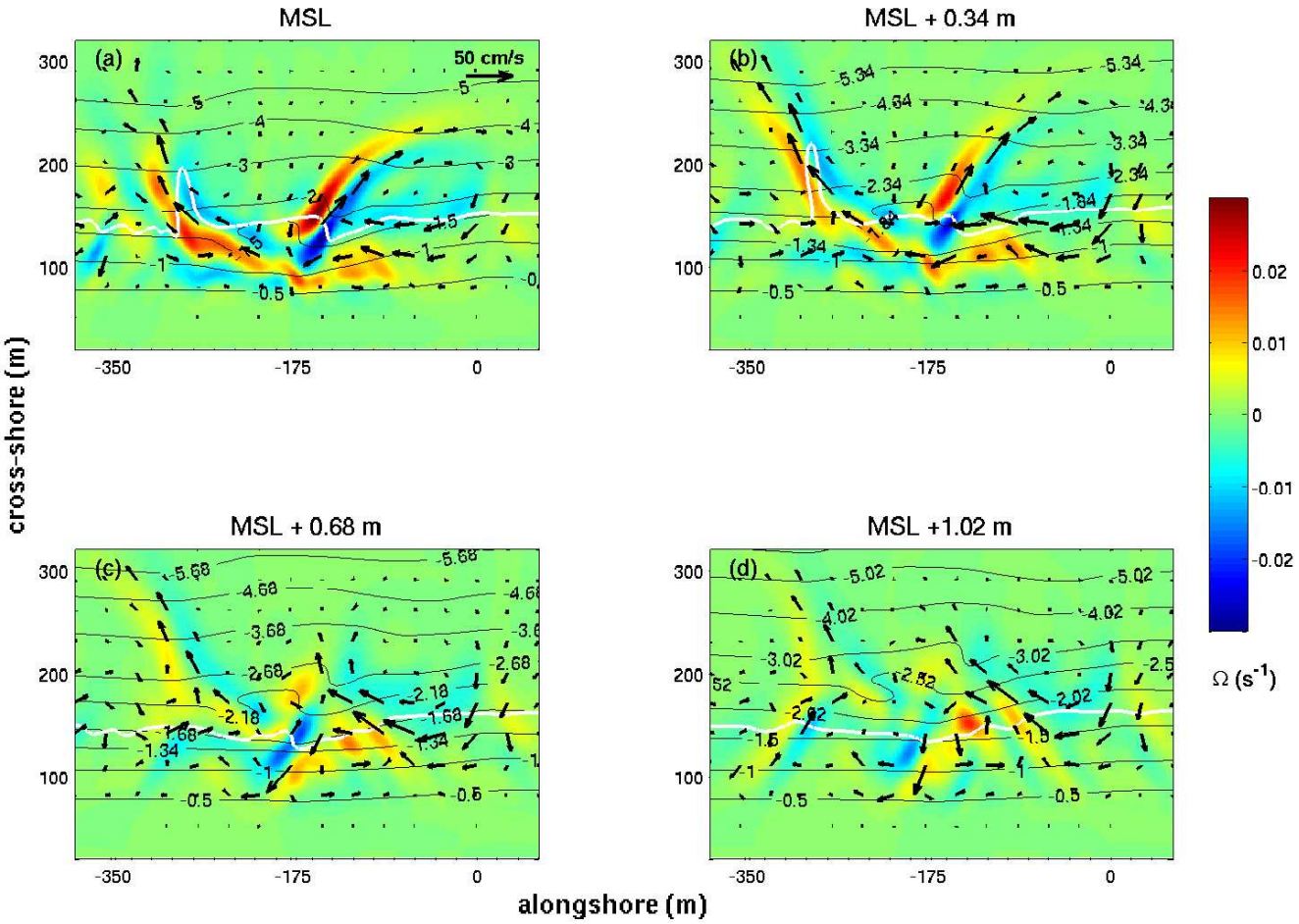

Figure 13. Case 2 2-hr mean model vorticity (color) and velocity (arrows) for tide levels of (a) MSL, (b) MSL + 0.34 m, (c) MSL + 0.68 m, and (d) MSL + 1.02 m.

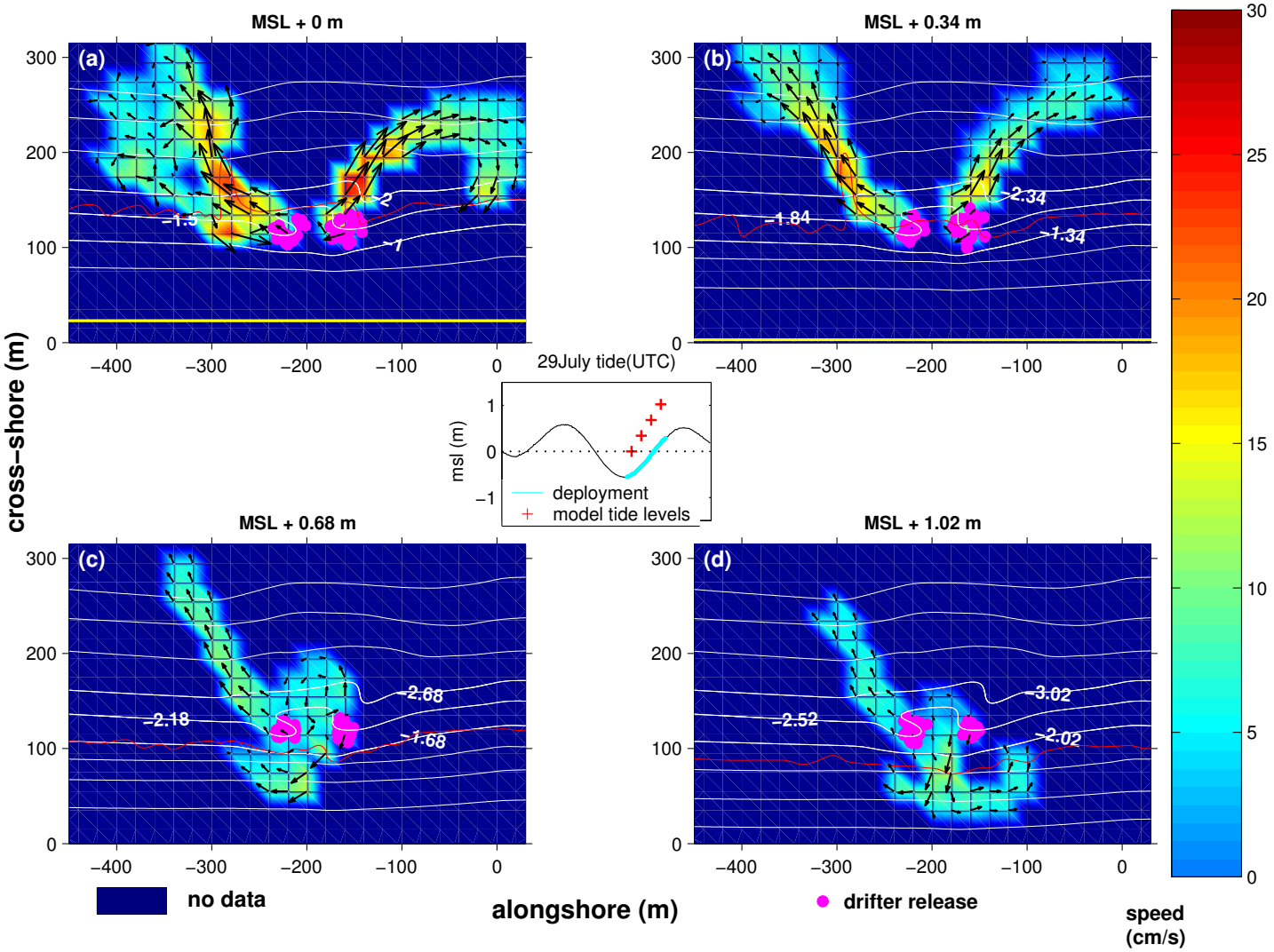

Figure 14. Simulated Case 2 spatially and temporally averaged drifter velocities. See Figure 6 format. Tide levels are (a) MSL, (b) MSL + 0.34 m, (c) MSL + 0.68 m, and (d) MSL + 1.02 m. Center panel shows tide level for UTC 29 July 2002 (thin black curve), mean tide level of the Case 2 observations (cyan curve), and the discrete tide levels of the present Case 2 simulations (asterisks).

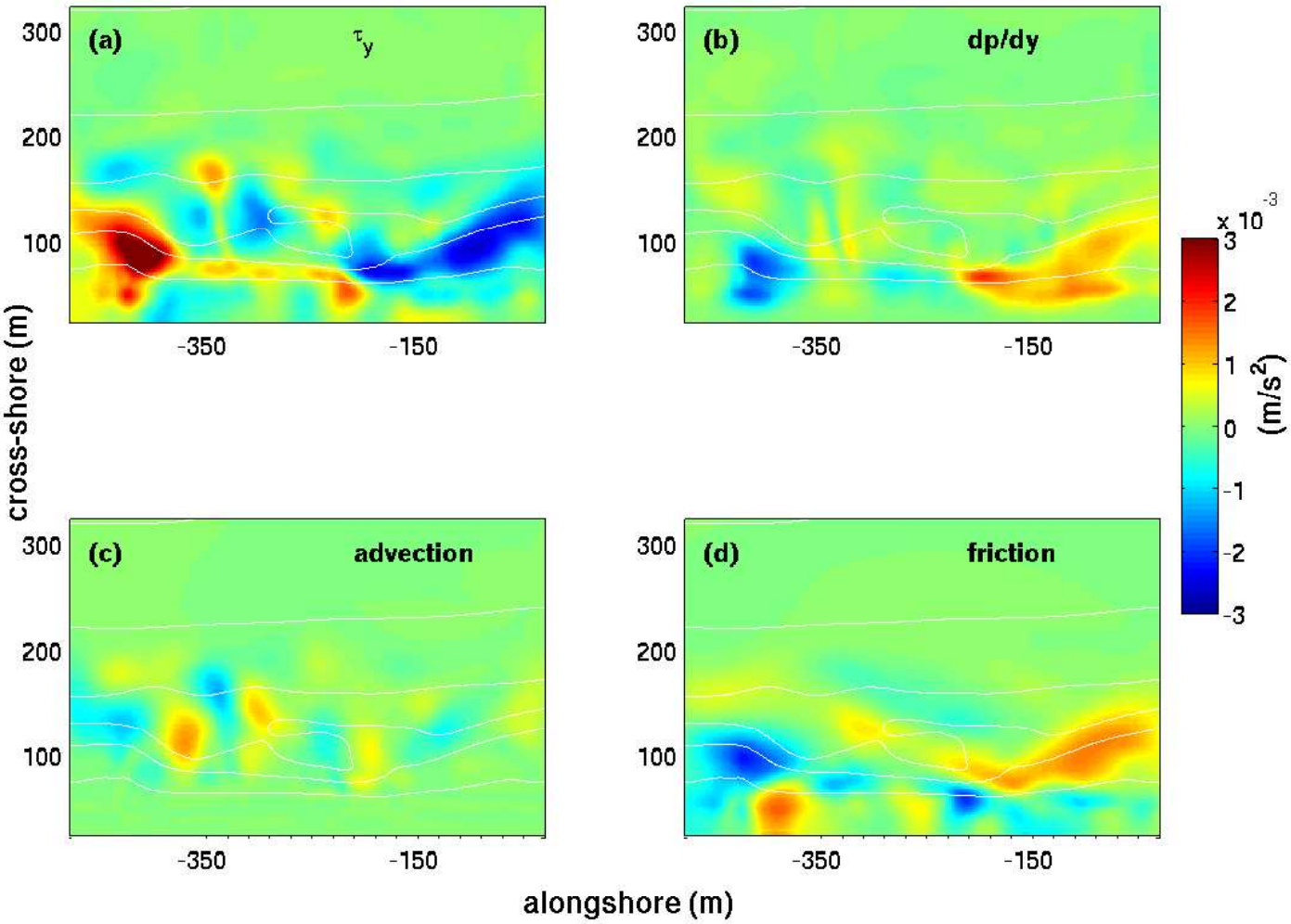

Figure 15. Case1 time mean (2 hr) alongshore momentum balance terms for tide level of MSL. (a) Wave forcing (τ_y), (b) pressure gradient (dp/dy), (c) advection, and (d) friction. Color scale at right. White curves are bathymetric contours. Biharmonic dissipation and residual terms were negligible.

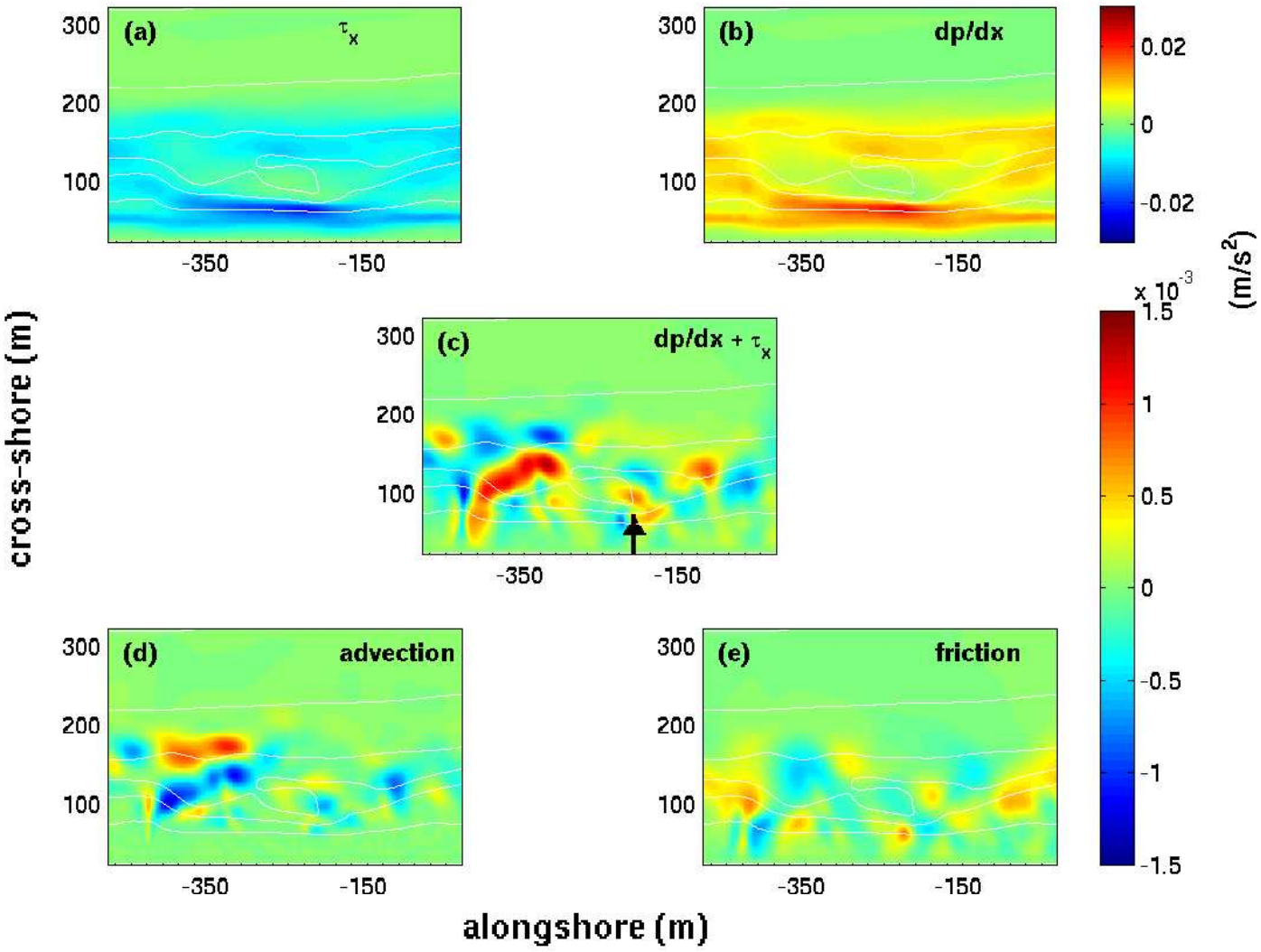

Figure 16. Case 1 mean (2 hr) cross-shore momentum balance terms for tide level of MSL: (a) Wave forcing (τ_x), (b) pressure gradient (dp/dx), (c) sum of dp/dx and τ_x, (d) advection, and (e) friction. The color scales at right (upper (a, b), lower (c, d, e)) differ by about a factor of 10. White curves are bathymetric contours. Black arrow in (c) indicates feature discussed in text. Biharmonic dissipation and residual terms were negligible.

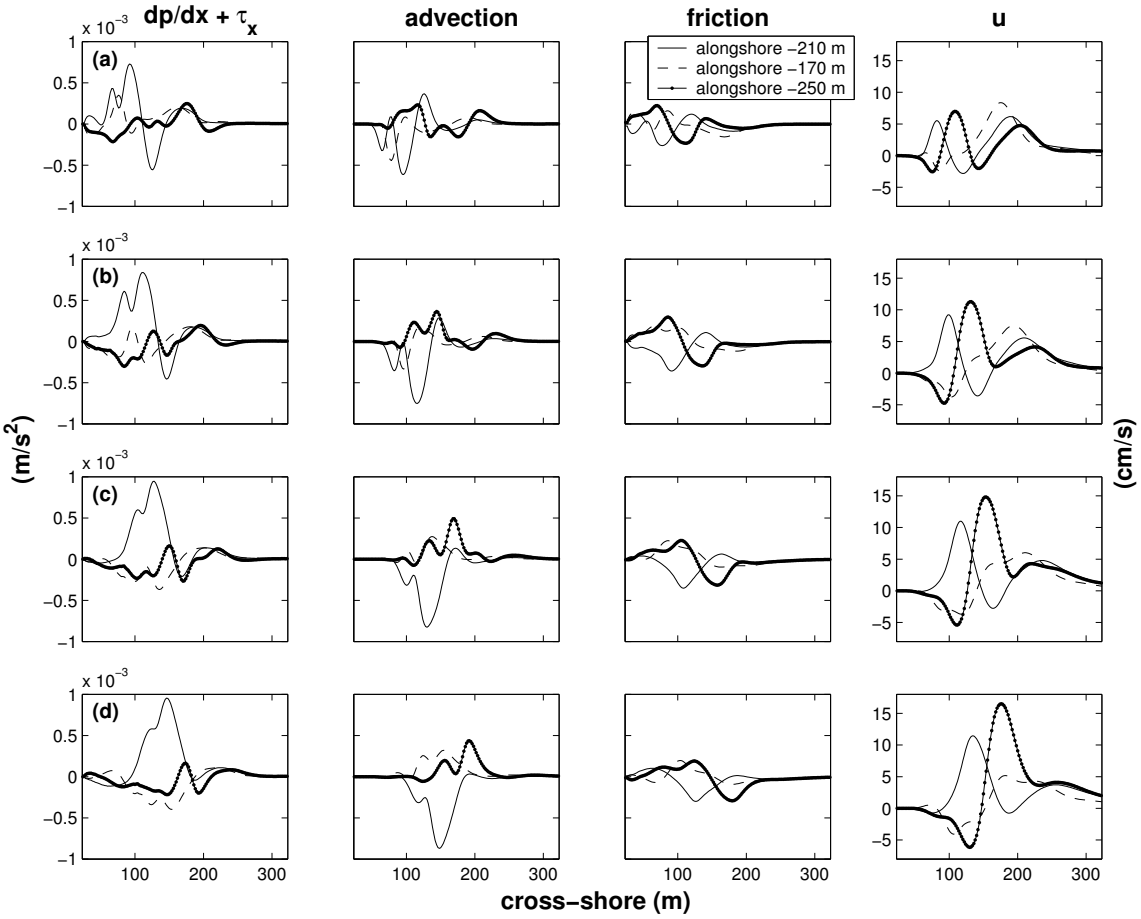

Figure 17. Case 1, 2-hr mean x-momentum balance terms (left 3 columns) and cross-shore velocity **u** (right column) versus cross-shore position at selected alongshore locations for tide levels of (a) MSL, (b) MSL + 0.34 m, (c) MSL + 0.68 m, (d) MSL + 1.02 m.